# Competition of spin-flip and spin-flop dominated processes in magnetic multilayers: Magnetization reversal, magnetotransport, and domain structure in the NiFe/Cu system

D. Elefant,* R. Schäfer, J. Thomas, and H. Vinzelberg
*Leibniz-Institut für Festkörper und Werkstoffforschung IFW Dresden, D-01069 Dresden, Germany*

C. M. Schneider
*Institut für Festkörperforschung IFF-9, Forschungzentrum Jülich, D-52425 Jülich, Germany*
*and Center of Nanoelectronic Systems for Information Technology (CNI), Research Centre Jülich, D-52425 Jülich, Germany*
(Received 1 September 2007; published 18 January 2008)

Changes in the magnetization structure of an antiferromagnetically (afm)-coupled metallic multilayer as a function of the applied field $H$ along the easy axis may involve both spin-flip and spin-flop events. The latter are widely discussed as the origin of the characteristic shapes of the magnetization $M(H)$ and giant magnetoresistance (GMR) curves. In this work, we demonstrate the influence of spin-flip processes, which result in very different magnetization reversal and resistivity characteristics as compared to the spin-flop case: sharp, steplike GMR and magnetization changes for both the surface and internal layers—including magnetic viscosity effects—are observed. By means of Kerr microscopy, Kerr magnetometry, GMR, and magnetization measurements we show that spin-flip transitions via domain wall displacement constitute the relevant mechanism of magnetization reversal, provided that the anisotropy field $H_K$ in the multilayer surpasses the antiferromagnetic coupling field $H_{afm}$. In this case, a linear dependence of the GMR on the magnetization is observed, whereas for fields applied along the hard axis magnetization rotation results in a quadratic dependence. The strong change of the ratio $H_K/H_{afm}$ could be realized for measuring temperatures between 4.2 and 470 K in a series of wedge-type NiFe/Cu multilayers prepared by dc magnetron sputtering and showing GMR amplitudes of up to 12% (300 K) and 28% (4.2 K) in the second afm coupling maximum with extremely low values of the afm coupling strength.

DOI: 10.1103/PhysRevB.77.014426 PACS number(s): 75.75.+a, 73.50.Jt, 75.60.Jk, 75.60.Ch

## I. INTRODUCTION

In magnetic multilayers (MLs) consisting of ferromagnetic (fm) layers that are interspaced by nonmagnetic layers we encounter a complicated interplay of competing interactions. Among others, these include the intralayer uniaxial magnetic anisotropy, the interlayer antiferromagnetic (afm) or fm coupling strength (depending on the nonmagnetic interlayer thickness), and the Zeeman energy in applied magnetic fields. This competition gives rise to a variety of peculiar magnetic properties, especially concerning the magnetization structure and hence also the giant magnetoresistance. Additionally, coercivity effects superimpose these interactions and the anisotropic magnetoresistance (AMR) contributes to the overall magnetoresistive behavior. Disentangling this interplay and discriminating the individual contributions is one of the major challenges in the study of multilayered systems.

In general, the most interesting case is that of an afm-coupled multilayer system, when the external field $H_a$ is applied parallel to the easy axis, along which the magnetization of the layers is stabilized by the anisotropy field $H_K$—orienting themselves in an alternating parallel and/or antiparallel scheme driven by the antiferromagnetic coupling field $H_{afm}$. Starting from this ground state, upon increasing $H_a$ a spin-flop motion of the fm layers is predicted to occur on the basis of calculations.[1] It is experimentally found[2,3] in the magnetization characteristics as a more or less sudden increase of the net magnetization above a certain field value $H_a$. The finite size of the MLs (normally the number $N$ of the ferromagnetic layers is less than 50 with an individual layer thickness in the nanometer range) leads to a nonuniform magnetization canting of the magnetic layers, because the surface layer is antiferromagnetically coupled to only one adjacent layer (theoretically shown for the isotropic case $H_K=0$ in Ref. 4). For the anisotropic situation, i.e., $H_K \neq 0$ the surface layer (in analogy to bulk antiferromagnets)[5] should already start to flop at a lower applied field than the bulk of the ML[2,3]—and with increasing $H_a$ these surface-flopped states should penetrate into the bulk of the ML. In this way a complicated nonuniform spin structure can evolve depending on $H_a$, the ratio $H_K/H_{afm}$, and $N$ (even, odd).[2,3,6] The complexity of the magnetization arrangement in the layer stack increases in the presence of biquadratic (90°-type) coupling.[7–9] This scenario is valid for the case $H_K < H_{afm}$, where

$$H_K = 2K/(\mu_0 M) \tag{1}$$

and

$$H_{afm} = 4J_{bil}/(\mu_0 M t) \tag{2}$$

with $K$ being the uniaxial (in some cases fourfold) anisotropy constant, $M$ the saturation magnetization of the fm component, $t$ the thickness of the fm layers, and $J_{bil}$ the bilinear coupling energy (see, e.g., Ref. 9; we neglect here biquadratic coupling contributions). Notice that in Eqs. (1) and (2) and in the following ones the defining relation $B=\mu_0(H+M)$ is used.

 

What happens, however, if the magnetic anisotropy field $H_K$ approaches and exceeds $H_{afm}$, i.e., if

$$H_K \geqslant H_{afm}, \quad K \geqslant 2J_{bil}/t. \tag{3}$$

This is also a very peculiar and interesting case, which we have decided to address with the present work. The aim of this work is to show the following.

(1) Depending on the increasing ratio $H_K/H_{afm}$ in finite size multilayers there is a transition to a spin-flip magnetization reversal process in applied fields (calculated in Ref. 1 for infinite MLs; experimentally stated only for epitaxially grown bilayers, e.g., Refs. 10 and 11).

(2) The spin-flip transitions remarkably influence the giant magnetoresistance (GMR) characteristics.

(3) There is a finite size effect, i.e., a difference in spin-flip switching fields between the surface layer and the bulk of a multilayer.

In order to substantiate these statements we need dedicated samples. With respect to a high GMR signal the Fe/Cr, Co/Cu, and $Ni_{80}Fe_{20}$/Cu multilayer systems are the most interesting ones. It is difficult, however, to drive the magnetic anisotropy beyond the afm coupling strength without at the same time decreasing the GMR in these systems. We found a possibility to fulfill the condition given in Eq. (3) by preparing $Ni_{80}Fe_{20}$/Cu multilayers in the second afm coupling maximum (very small $J_{bil}$) and moderately thick $Ni_{80}Fe_{20}$ layers with $t \cong 2$ nm.

In the following we will first describe the results of experiments performed by means of superconducting quantum interference device (SQUID) magnetometry, alternating gradient magnetometry (AGM), and GMR studies in the temperature range $T=4-470$ K, and complemented by Kerr microscopy and Kerr magnetometry [magneto-optical Kerr effect (MOKE)] at room temperature. The combination of these techniques allows us to obtain a detailed picture of the microscopic and depth-dependent magnetization reversal processes in the multilayer structure.

## II. PREPARATION

A series of $Ni_{80}Fe_{20}$/Cu multilayers (for reasons of brevity, we will use NiFe in the following to denote Permalloy with the composition $Ni_{80}Fe_{20}$) with wedge-shaped Cu and NiFe layers (Fig. 1) was grown by dc magnetron sputtering onto thermally oxidized Si wafers in an Ar atmosphere (for preparation details, see Ref. 12). The thickness of the Cu wedge ranged from 2.4 to 1.9 nm, thus enclosing the second afm coupling maximum between fm coupling thickness regions on a single wafer, as it is shown by the corresponding Kerr images in Fig. 1. Across the wedge direction, 1 mm wide and 15 mm long four-toothed comb structures were photolithographically etched out of the continuous multilayer stack for four-point dc measurements. The geometry of the comb etching masks on top of the layer stack is sketched in Fig. 1. On the one hand, this sample geometry allowed us to perform GMR, Kerr microscopy, and MOKE measurements on the very same comb between the potential contacts, whereas for the magnetization measurements (SQUID and AGM) adjacent $3\times1$ mm$^2$ pieces from the same stripe were

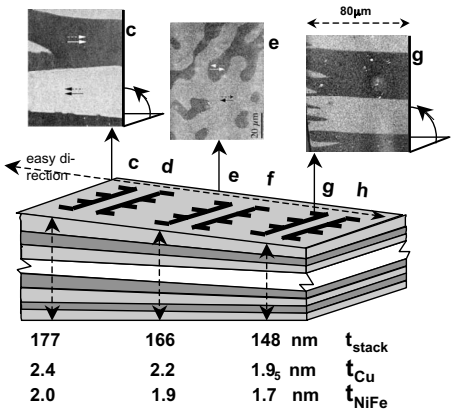


FIG. 1. Scheme of the wedge shaped NiFe/Cu multilayer $40\times[\mathrm{NiFe}(t_{\mathrm{NiFe}})\mathrm{Cu}(t_{\mathrm{Cu}})][\mathrm{NiFe}(t_{\mathrm{NiFe}})]$ with sample arrangement on the wafer. The geometry of the four-toothed combs, which are photolithographically etched out of the layer stack, is depicted by the solid line structures on the top layer. The individual combs are marked by letters for later reference. For combs c, e, and h the thickness of the layer stack $t_{stack}$ and the thicknesses of the Cu and NiFe single layers are denoted and related Kerr images are shown (note that the $z$ direction is scaled by orders of magnitude; the lateral dimensions are $\approx 20\times60$ mm$^2$).

cut. On the other hand, the rather large comb width helped us to reduce parasitic shape anisotropy effects, which had been observed in stripes with smaller width.[13] The samples in the afm coupling regime showed GMR amplitudes of up to 50% (at $T=4.2$ K) and 25% (at 300 K) in the first afm coupling maximum and up to 28% (4.2 K) and 12% (300 K) in the second afm coupling maximum, respectively. In the following, only the samples with interlayer thicknesses around the second afm coupling maximum will be considered, because they reveal extremely low coupling constants $J_{bil}$ and afm coupling fields $H_{afm}$, respectively. In order to distinguish "bulk" and "surface" layers the stacks under consideration had a total thickness of about 160 nm and a nominal structure $40\times[\mathrm{NiFe}(t_{\mathrm{NiFe}})\mathrm{Cu}(t_{\mathrm{Cu}})]$ $\mathrm{NiFe}(t_{\mathrm{NiFe}})$ with a wedge-type thickness variation $t_{\mathrm{NiFe}}=1.7-2$ nm and $t_{\mathrm{Cu}}=1.9-2.4$ nm, respectively. To avoid parasitic effects we omitted any buffer and cap layers. Figure 1 shows a sketch of the comb arrangement on the wedge. The Kerr images, obtained after an ac demagnetization procedure, demonstrate the fm-afm-fm coupling transitions and prove that the magnetic easy axes are oriented along the wedge direction. Irregular patch domains are found for afm coupling (comb e), whereas straight 180° domain walls are dominant for fm coupling. Similar domains have also been observed in trilayer systems.[7,14,15]

In order to change the ratio $H_K/H_{afm}$ continuously over a wide range in one and the same sample (based on different temperature characteristics of $H_K$ and $H_{afm}$) the measurements covered the temperature range $T=4.2-470$ K. To ensure reproducible data for the temperature cycling in this range, the samples were vacuum annealed ($p \cong 10^{-4}$ Pa) for 1 h at 200 °C. This procedure additionally resulted in a small increase of the GMR (also reported in Refs. 16 and 17). In Ref. 18 it was concluded from a decreasing linewidth of the ferromagnetic resonance that this treatment reduces

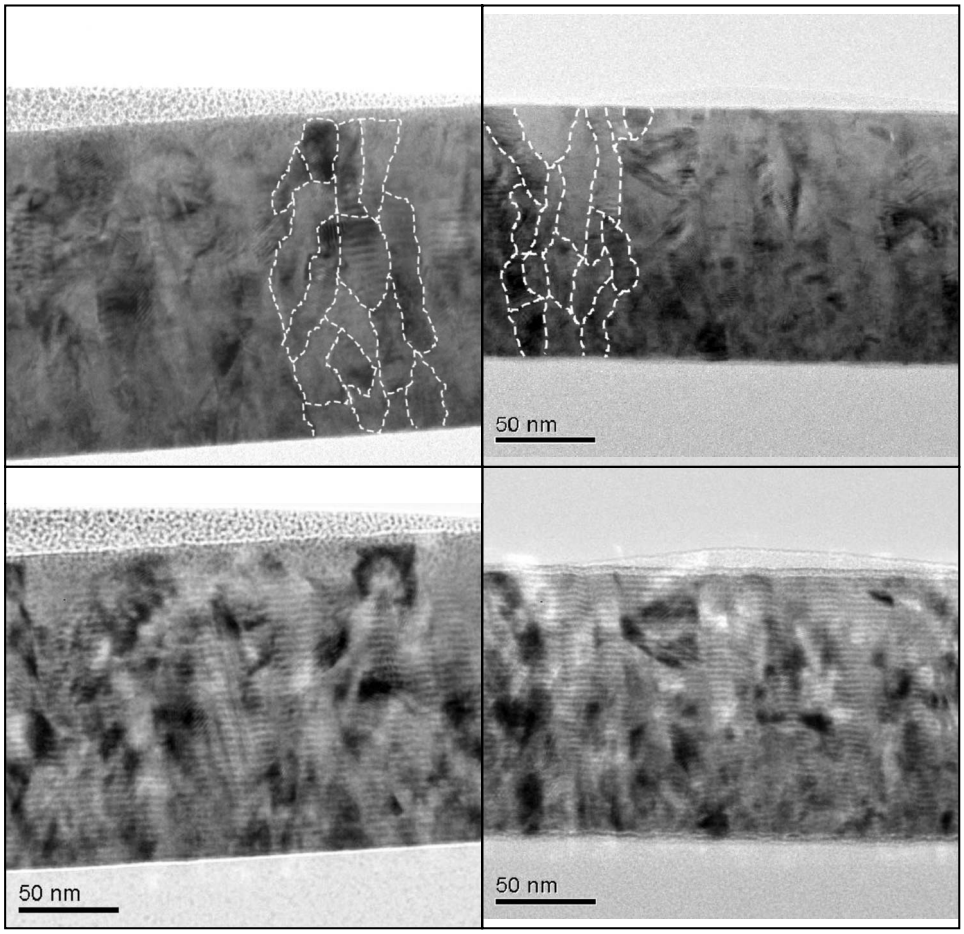


FIG. 2. TEM cross section images of the NiFe/Cu multilayers. Left side: afm-coupled sample (comb f in Fig. 1); right side: fm-coupled sample (comb h in Fig. 1). Top images: focused regime; bottom images: defocused regime. The broken lines are guides for the eyes and follow the grain boundaries.

the defects and improves the magnetic homogeneity of the multilayer stack.

## III. EXPERIMENTAL RESULTS AND DISCUSSIONS

### A. Structural aspects

The structure of the multilayers was characterized by transmission electron microscopy (TEM) cross section investigations after preparation by a focused ion beam technique. Figure 2 shows images of an afm-coupled (comb f in Fig. 1) and an fm-coupled sample (comb h). The focused images reveal the MLs to consist of columnar single crystalline grains, coherently grown through partly more than 20 Cu/NiFe double layers up to 20 nm in diameter. In contrast to this, the defocused images emphasize the layer structure. No significant difference in the microstructure between the antiferromagnetically and ferromagnetically coupled MLs is found on this level. X-ray wide angle diffraction patterns taken from unstructured reference multilayer samples, which have been prepared in parallel (not shown here, compare Ref. 17), display a ⟨111⟩ texture of the columnar crystallites. The surface topography has been determined by atomic force microscopy measurements, which yield a rms roughness of $\leqslant$0.8 nm at the surface of the 166 nm thick layer stack.

### B. Anisotropy in the ferromagnetic region and mean anisotropy field $H_K$

In afm-coupled multilayers the magnetic anisotropy and the antiferromagnetic coupling are superimposed, thus posing a problem to their quantitative separation. Therefore, the magnetic anisotropy should be estimated more reliably from measurements in the ferromagnetic coupling regime. Figure 3 shows the room temperature magnetization loops for fm-coupled samples on both sides of the wedge (combs c and h, Fig. 1) for the easy and hard directions, respectively, indicating a pronounced anisotropy in small fields. The origin of this anisotropy in Permalloy films was already intensely and controversially discussed in the 1950s and 1960s as (i) a directional atom-pair (Fe-Fe) ordering mechanism like that found in bulk alloys (for a review, see Ref. 19), and (ii) a growth-induced shape anisotropy, being due to the crystalline microstructure of the films and the associated dipolar field distribution (for a summary of the arguments and references, see Ref. 20). Note that the magnetocrystalline anisotropy and

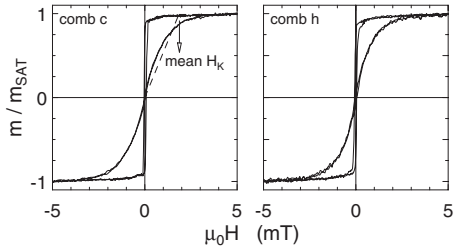


FIG. 3. Magnetization loops of the ferromagnetic coupling samples on the wedge (comb c and h, Fig. 1) for the applied field along the easy and hard directions, respectively, $T$=300 K.

TABLE I. Average anisotropy fields $\mu_0 H_K$ (mT) for ferromagnetically coupled multilayers on the wedge (see text and Fig. 1).

| Temperature | 50 K | 100 K | 200 K | 293 K | 390 K | 473 K |
|---|---|---|---|---|---|---|
| Comb c | $2.0_2$ | $1.9_8$ | $1.9_0$ | $1.8_7$ | $1.7_9$ | $1.7_7$ |
| Comb h | $1.8_0$ | $1.7_9$ | $1.7_0$ | $1.6_7$ | $1.5_5$ | $1.4_0$ |

the magnetostriction nearly vanish in Permalloy. The anisotropy fields of our multilayers (see Table I) exceed those published for the pair-ordering mechanism for both evaporated[19] as well as sputtered[21] Permalloy films, by a factor of 4–10. Therefore, we conclude that the pair-ordering model will not be the dominant reason for the anisotropy in our material.

Recalling the crystalline microstructure of our samples and following the arguments and equations in Ref. 22 we propose the following model for the magnetostatic energy due to free poles in a magnetically inhomogeneous material: The cross sections of the columnar grains, shown in Fig. 2, are somewhat elongated (i.e., elliptically shaped) in the wedge direction due to the sputtering process taking place at oblique incidence. In the grain boundaries lattice defects, impurities, and Ni-Fe stoichiometry fluctuations give rise to small local modifications of the magnetization compared to the single crystalline grains. As a consequence, free poles will appear at the grain boundaries and hence in every crystallite $i$ with volume $dV$ a small shape anisotropy energy contribution

$$K_i dV = \frac{1}{2\mu_0} \Delta N_i \cdot (\Delta \mu_0 M_i)^2 dV \tag{4}$$

will be created. In Eq. (4) $\Delta N$ denotes the difference of the demagnetizing factors in the long and short directions of the cross section of the columnar grain and $\Delta M$ is the difference of the magnetizations of the single crystalline grain and the grain boundary region, respectively. A relation of this type is also given in Ref. 22 for elongated magnetic precipitations having a different magnetization than the magnetic matrix.

For this case Eq. (1) is modified to $H_K = 2K/(\mu_0 \Delta M)$ and with Eq. (4) follows for the shape anisotropy field $H_{K,i}$ in the grain $i$

$$H_{K,i} = M \cdot \frac{\Delta M_i}{M} \cdot \Delta N_i. \tag{5}$$

The area between the magnetization loops for the easy and hard directions corresponds to the anisotropy constant $K$.[23] Integrating in this way over the loops in Fig. 3 one arrives at a grain-averaged version of Eq. (4) and thus a grain-averaged anisotropy constant $K$. With the help of Eq. (1) one obtains the anisotropy field $H_K$ as the average of the $H_{K,i}$ distribution in the grains. Figure 4 reveals the temperature dependence of the hard axis magnetization loops to be very small, hence the mean anisotropy field $H_K$ depends only marginally on the temperature. In Table I the mean $H_K$ values—computed from the magnetization loops—for combs c and h (see Fig. 1) on both sides of the wedge are compiled for the temperature range $T = 50-470$ K. The corresponding anisotropy fields for the afm-coupled comb e should be found in between these values. The observed range of $\mu_0 H_K \leqslant 2$ mT shows that in our model only a few percent of ellipticity (the $\Delta N$ values for elliptic cross sections in elongated ellipsoids are given in Ref. 24) as well as in the magnetization modulation between grains and grain boundaries are required to reproduce these $H_K$ values according to Eq. (5) with the saturation magnetization $\mu_0 M \cong 1$ T in Permalloy.

### C. Giant magnetoresistance anisotropy in the afm-coupled region

In Fig. 5 we show the resistivity and the magnetoresistance $\mathrm{GMR} = [\rho(H) - \rho(H_{sat})]/\rho(H_{sat})$ with $\mathrm{GMR}_{max} = [\rho(H=0) - \rho(H_{sat})]/\rho(H_{sat}) = 12\%$ at room temperature for the afm-coupled wedge region (Fig. 1, comb e). We find drastically different characteristics when the field is applied along the easy and hard directions, respectively. For the hard direction the well-known continuous and broad triangular GMR curve due to magnetization rotation processes is reproduced, whereas for the easy direction a discontinuous field dependence shows up. The plateaulike behavior at higher fields is followed by a sudden resistivity breakdown for very small field changes around $\mu_0 \cong 1$ mT, which can only be explained by micromagnetic processes involving domain wall displacement. Also, an additional structure at somewhat higher fields is visible in the curve.

Let us take a closer look at the easy axis curve in Fig. 6, paying particular attention to time-dependent effects. The regular measuring procedure for the resistivity is as follows: The applied field is changed by a small increment and then at constant field the voltage drop across the sample is measured

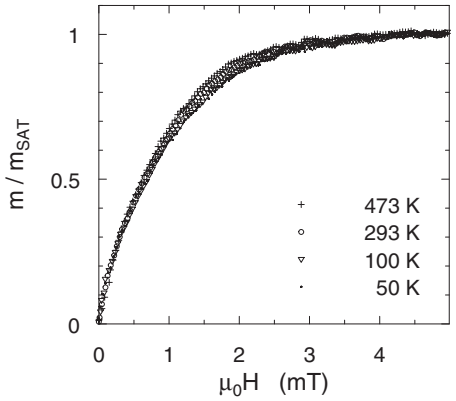


FIG. 4. Normalized magnetization along the hard direction for different temperatures (comb c, Fig. 1).

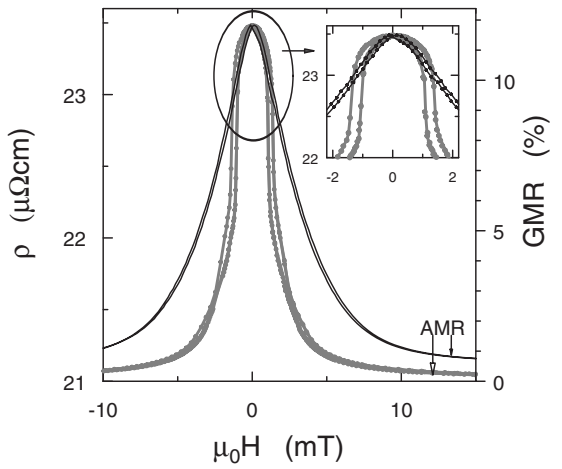


FIG. 5. Variation of the GMR with the external field applied along the easy axis (gray) and along the hard direction (black) for an afm-coupled sample (comb e, Fig. 1). The inset shows the low field region in detail.

at a constant dc during a preset amount of time (usually some seconds), followed by the next incremental field change. In Fig. 6 these measured points are connected by full lines. In a different technique, at some (arbitrary) applied field values the resistance measurements are repeated after some time (1–100 min) without incrementally changing the applied field. The repeated measurements deliver a time-dependent variation of the resistivity. These points are not connected by lines and form gaps in Fig. 6.

The occurrence of these gaps in the resistance curves is related to time-dependent resistivity changes and they suggest a magnetic after effect in the magnetization structure of

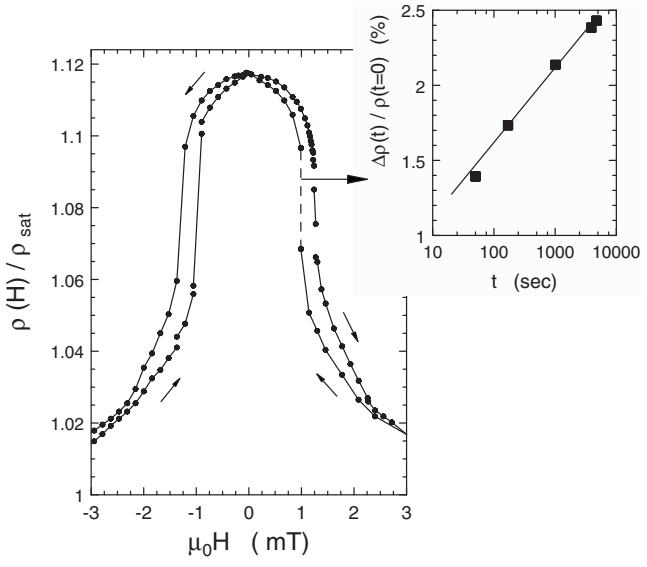


FIG. 6. Time-dependent GMR effects along the easy axis (compare Fig. 5). Experimental data points not connected by full lines ("gaps" in the GMR curve) represent measurement repetitions after some time (range of minutes) at constant field (see text). The inset shows the time dependence of the resistivity change for the largest gap (corresponding to the dotted line in the main figure).

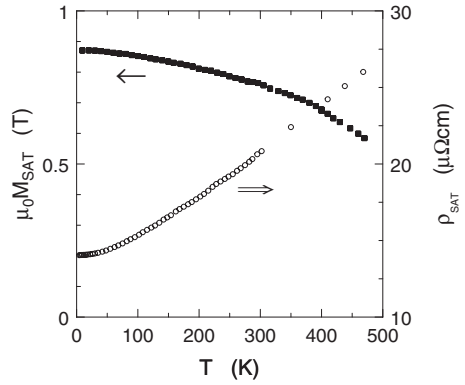


FIG. 7. Temperature dependence of the magnetization $M$ (■) and resistivity $\rho$ (○) of the afm-coupled ML in the saturated state (applied saturation field $\mu_0 H = 50$ mT).

the multilayer and hence also in the resistivity. The magnetic after effect (or magnetic viscosity) can have several reasons, but its main characteristic is a logarithmic time dependence of the magnetization within a "time window" $\Delta J \propto S \ln(t)$ with $J = \mu_0 M$ (for a short overview, see Ref. 25). For the largest gap (corresponding to 25% of the full GMR signal—the dotted line in Fig. 6) the inset in Fig. 6 shows the time dependence of the resistivity to fulfil this logarithmic dependence $\Delta\rho \propto \ln(t)$. In Ref. 26 a thermal fluctuation magnetic after effect for the domain wall displacement in magnetic films has been discussed. We suggest this mechanism to also be at work in our multilayers. In our case, a domain wall displacement will directly convert afm oriented areas into fm arranged ones [compare the sketch in Fig. 13(a)], and vice versa. Because the GMR can occur only in the afm layered volume fraction, a linear relation $\Delta\rho \propto \Delta M_{stack}$ is implied. In most of the cases observed—where an applied field causes magnetic layers to rotate against each other—no linear relationship $\Delta\rho \propto \Delta M_{stack}$ should be expected. For magnetic bilayers one often finds $\Delta\rho \propto \cos^2(\theta/2)$ with $\theta$ being the angle between the $M$ directions of the components (see, e.g., Refs. 27 and 28). This leads to a quadratic dependence $\Delta\rho \propto \Delta M^2_{stack}$.

In conclusion, we can state that the bulk of the ML switches at a field $H$ which we have to identify with the afm coupling field $\mu_0 H_{afm} \cong 1.1$ mT after Eq. (2), and which is smaller than the anisotropy fields $H_K$ listed in Table I.

### D. Temperature dependence of magnetization and giant magnetoresistance

In the next step we turn to the temperature dependence of the saturation values of the magnetization $M_{sat}$ and resistivity $\rho_{sat}$ in the afm-coupled MLs. The data for the temperature range $T = 4$–$470$ K are shown in Fig. 7. The values of $M_{sat}$ are related to the nominal volume content of NiFe in the ML (see Fig. 1). Despite taking into consideration an eventual relatively large NiFe layer thickness error, the saturation magnetization $M_{sat}$ in our multilayers is lower than the values $\mu_0 M_{sat}(T \to 0) \cong 1.12$ T published for a 500 nm thick (single) Permalloy film.[29] The reduced values in our films

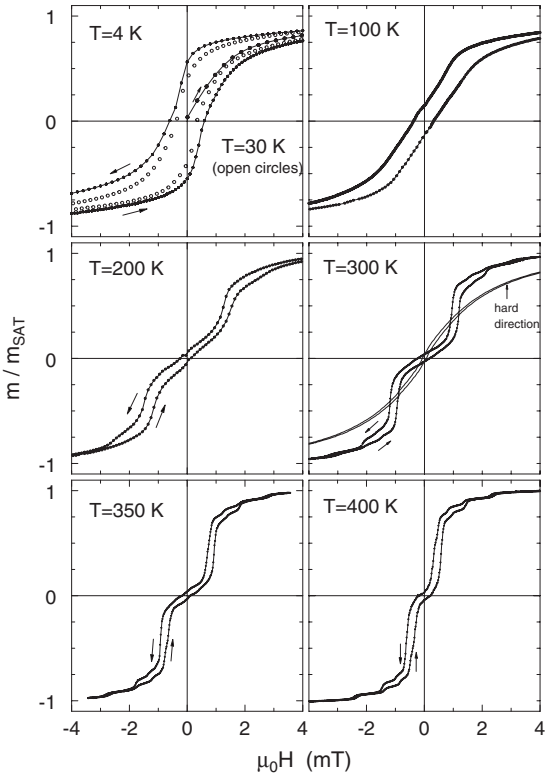


FIG. 8. Magnetization loops with $\vec{H}$ along the easy axis for temperatures in the range $T=4-400$ K (afm-coupled sample, comb e in Fig. 1). For $T=300$ K the loop for the hard direction is added. The loops are normalized to the saturation values (see Fig. 7).

could be ascribed to the high percentage ($\approx 20\%$) of interface lattice planes of the $\leqslant 2$ nm thick Permalloy layers. A discussion of the $T$ dependence of the saturation resistivity of MLs—including results on the NiFe/Cu system—is given elsewhere.[30] With Fig. 7 all the reduced $\rho$ and $M$ values mentioned in the remaining part of the paper can be transformed into absolute values.

In Fig. 8 we compile the magnetization loops for the easy direction in the afm-coupled region (comb e in Fig. 1) in the temperature range $T=4-400$ K. The characteristic loop at $T=300$ K directly reflects the peculiarities observed in the GMR curve of Fig. 5, especially the large drop in the field range around $\mu_0 H_{afm} \cong 1$ mT. Comparing the curves in Fig. 8 we can summarize the following: (i) Toward higher temperatures the jumplike character of the curves becomes more pronounced whereas the steps are shifted to lower field values. (ii) Toward lower temperatures a further increase of the afm coupling seems to occur, but the steps in the curves smooth out. (iii) At lowest temperatures the coercivity increases and dominates the magnetization loop.

Figures 9 and 10 show the temperature dependence of the GMR characteristics with a field applied along the easy direction. A very satisfactory agreement of the magnetization (Fig. 8) and GMR features can be stated. From room temperature toward low temperatures we observe at first the afm coupling field to increase, accompanied by a smoothing of the steps or kinks. This process is followed by a transition from the bell to a triangular shape of the curves, which are

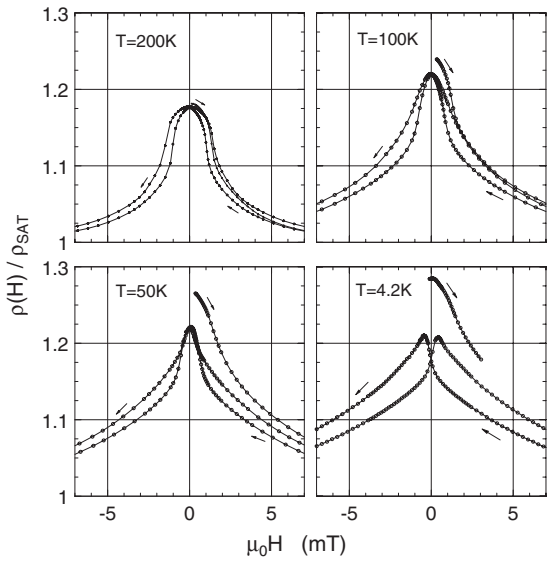


FIG. 9. GMR loops obtained from an afm-coupled multilayer (comb e in Fig. 1) for $H$ along the easy direction toward low temperatures. The branches starting from the demagnetized state are added.

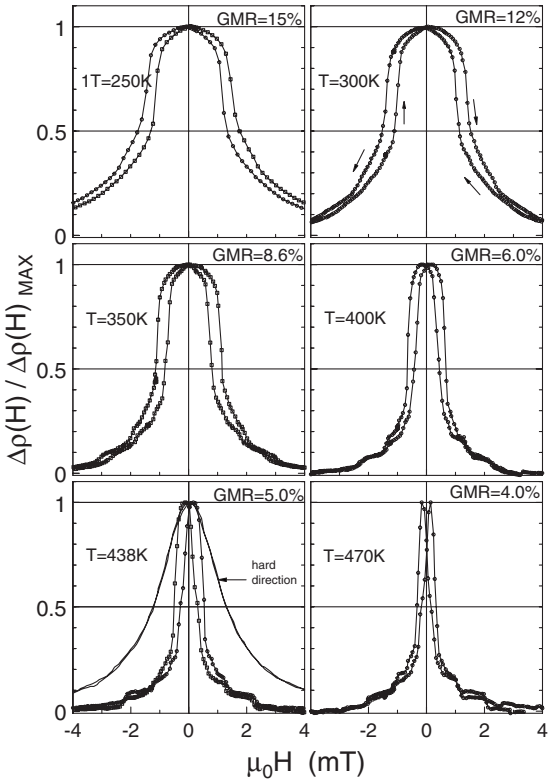


FIG. 10. GMR loops for an afm-coupled NiFe/Cu multilayer (comb e in Fig. 1) for $H$ along the easy direction for the temperature range $T=250-470$ K. The GMR values are normalized to the maximum GMR value at the corresponding temperature, which is denoted in every diagram. For $T=438$ K the hard direction loop is added.

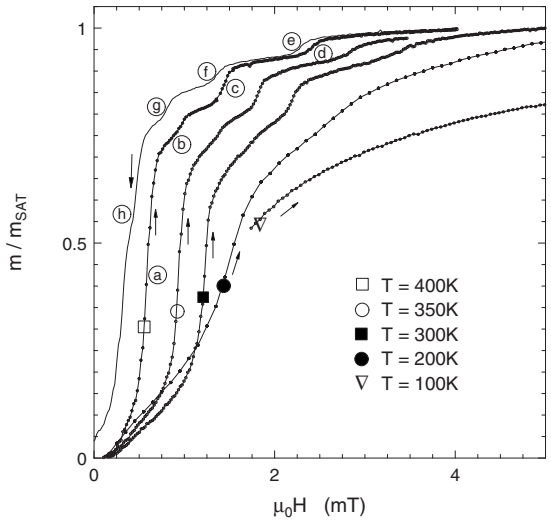


FIG. 11. The magnetization loop (ascending) branches in quadrant 4 (see Fig. 8) for different temperatures to show the increasing steplike character. For $T=400$ K quadrant 1 (descending) branch is added. The reason for the smaller magnetization jump at step "d" should be seen in the light of the discussion in Sec. III H and may be related to a nonideal switching taking place at $H_K < H_{afm}$.

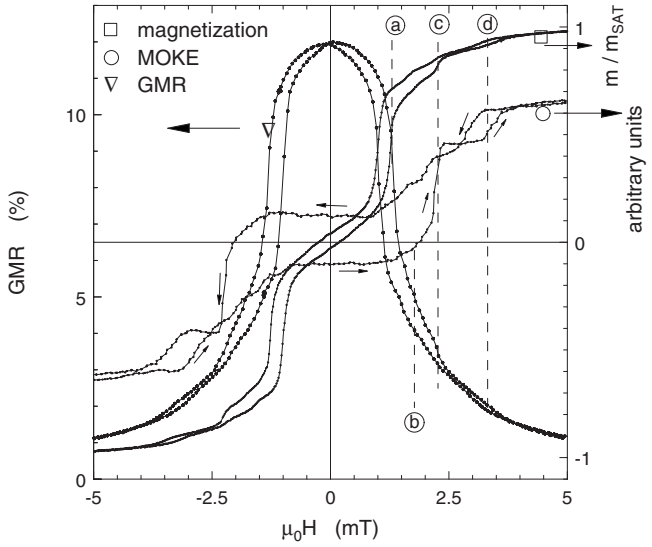


FIG. 12. GMR, magnetization, and MOKE loops for the afm-coupled ML with applied field along the easy axis at $T=300$ K.

more and more dominated by the increasing coercivity. This is clearly demonstrated, e.g., by the increasing difference between the resistivity values starting from the demagnetized state and the cycled curves, additionally developing a double peak. In this case, contrary to the findings at higher temperatures, only the height of the GMR effect, but not the shape of the magnetization and resistivity loops unambiguously reflects the afm coupling of the multilayer.

Toward higher temperatures, Fig. 10 shows an increasing steplike character of the GMR curves, especially for the peculiar steps at higher applied fields together with a shift of all steps to lower fields—in coincidence with the magnetization loops in Fig. 8. In Fig. 11 we just want to confirm this conclusion by showing for clarity only the branches in the last quadrant of the magnetization loops (ascending branches) from Fig. 8 for different temperatures.

### E. Combination of giant magnetoresistance, magnetization, magneto-optical Kerr effect, and Kerr microscopy results

For the further interpretation it is useful to combine the GMR characteristics, the magnetization loop, and the MOKE loop versus the applied magnetic field in the easy direction into a single graph (Fig. 12). These data were all measured on the afm-coupled sample (comb e in Fig. 1) at room temperature. GMR and magnetization, both being volume quantities, show large and small steps at identical magnetic field values. Especially the large and sudden changes, marked with encircled "a," suggest that the bulk of the ML stack switches at this field ($\mu_0 H \cong 1$ mT) from the afm-coupled state to the fm state and vice versa, with some hysteresis between forward and backward branches. MOKE as a surface sensitive method shows clearly at least two transitions at considerably larger fields. These transitions in the MOKE loop are also visible as small kinks in the GMR and magnetization characteristics (marked as encircled c and d in Fig. 12). This observation clearly proves that the outermost layers of the stack switch at higher fields than the bulk of the ML.

Kerr microscopy imaging delivers additional and important information with respect to the surface transitions. Figure 13 shows Kerr images for applied fields along the easy (a) and hard axes (b). The series of images in Fig. 13(b) demonstrates that by decreasing the magnetic field from negative (coming from the bottom in the figure) saturation typical patchlike afm domains are formed. Passing remanence and increasing the field in positive direction do not change the shape of the domains—the domain structure remains rather constant, whereas just the domain contrast varies with the field. The largest contrast is observed in zero field, where the magnetization in the domains is parallel and/or antiparallel to the easy axis and parallel and/or antiparallel to the chosen magneto-optical (m.o.) sensitivity direction. Angular deviations of the magnetization from the m.o. axis decrease the contrast. All the observations listed above reveal (magnetization) rotation to be the mechanism of the magnetization reversal in applied fields—the arrows in the figure, showing the local magnetization directions, and the schematic drawings demonstrate this rotation.

A rather different process is shown in Fig. 13(a) with the field applied along the easy direction. Starting from the saturated state (following and comparing the loops in Fig. 12—especially the MOKE loop—and beginning with negative applied fields) the series in Fig. 13(a) starts (from below) with an image at $H=0$. The magnetic layers of the ML are now arranged in an antiparallel (afm) configuration. This can be concluded from the magnetization loop in Fig. 12, which shows a small remanence in direction of the previously applied field, due to the odd number of magnetic layers in the stack. The bottommost image shows a single domain surface

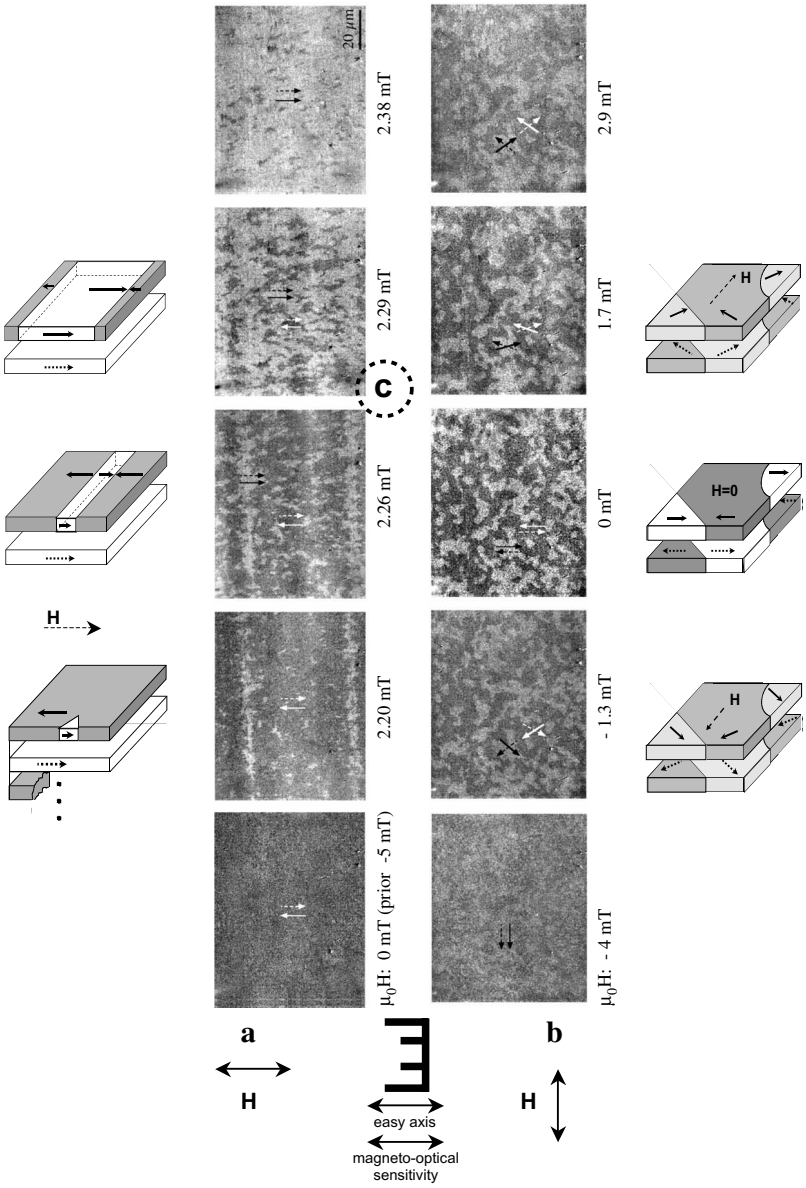


FIG. 13. Kerr microscopy images for the applied field $H$ along the easy direction (a) and along the hard direction (b) for the afm-coupled NiFe/Cu ML (comb e in Fig. 1). The arrows denote the magnetization direction: full arrows for the surface layer and dotted arrows for the next magnetic layer (see also the sketches). White and black arrows are only taken for contrast to the chosen surface area, where the arrows are situated. Compare the encircled "c" with the corresponding "c" line in Fig. 12 and see text.

state at zero field. Increasing the field above $\mu_0 H \cong 2$ mT in positive direction leads to a nucleation of domains, which are magnetized in the field direction (second image, bright areas). Further marginal increase of the field causes the main part of the observed layer to switch into the field direction within a small interval of only $\Delta H \leqslant 0.3$ Oe (see images 3 and 4). In contrast to Fig. 13(b) these images reveal domain wall displacement to be the dominating switching mechanism (at least) of the surface layer in an easy axis field. Comparing the field strength of this surface transition with the loops in Fig. 12, one can indeed identify this switching process with the peculiarities along line c in the figure. For MOKE as a surface sensitive method the loop shows a large jump, whereas the distinctly smaller effects in the loops of GMR and magnetization as bulk-related quantities indicate that the discussed transition is more or less limited to the surface region. A further somewhat smaller jump at higher fields in the MOKE loop is not clearly visible by Kerr microscopy, but discernable in the GMR and magnetization loops (see line d in Fig. 12). Its appearance suggests that this switching is located in a layer close to the surface. A third transition—clearly identified at point b in Fig. 11, and smeared out, but still visible in the MOKE loop at line b in Fig. 12—should be located in a layer somewhat deeper in the stack toward the bulk. It should be noted here that the information depth of the Kerr effect is about 20 nm in metallic systems, connected with an exponential decrease of the signal with the depth.[31] However, digitally enhanced Kerr microscopy relies on the (weak) Kerr contrast that is detected by a (in our case) regular video-rate charge-coupled device camera with moderate sensitivity. Therefore the signal-to-noise ratio of Kerr microscopy is reduced as compared to the higher sensitivity of an optical magnetometer, and it is mainly the outermost layers of the multilayer stack that contribute to the main contrast in Kerr images. For this reason the smaller magnetization jumps, still detectable by MOKE magnetometry, are hardly seen in the Kerr images (by using a phase-shifting optical compensator it would in principle be possible also to detect deeper layers within the information

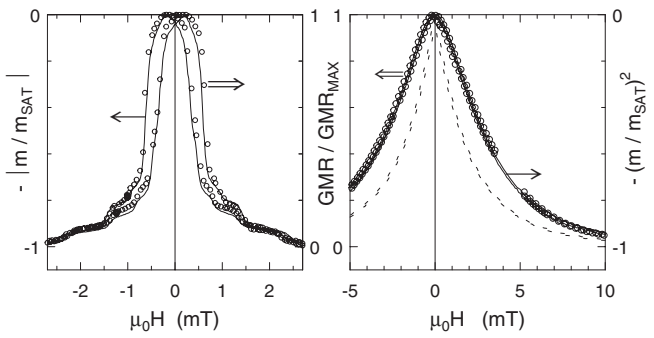


FIG. 14. Normalized GMR and normalized magnetization with $H$ along the easy direction (a) and GMR and quadratic magnetization along the hard direction (b). The open circles are measuring points of the GMR, whereas the full lines represent the magnetization results with a large number of data points. In (b) for $\mu_0 H \approx 5$ mT some GMR points are omitted to show the underlying magnetization values. The dotted line in (b) shows the magnetization for a linear $y$ scale as in (a).

depth limit[14]—this option, however, was not applied in the present work).

The bulk of the ML clearly switches at line a in Fig. 12. No peculiarities can be discerned for fields below the bulk switching field in any of the loops.

### F. Influence of switching type on relationship between giant magnetoresistance and magnetization loops

A change of the net magnetization of the ML by magnetization rotation or domain wall displacement should cause different functional relationships between the GMR and magnetization curves, as discussed above. Figure 14 shows that for magnetic fields applied along the easy direction indeed a linear connection between GMR and magnetization change is found, whereas for $H$ along the hard direction the GMR depends quadratically on the magnetization. Therefore, we can state that—in connection with the observed magnetic viscosity effects—along the easy direction the entire ML stack switches via a spin-flip mechanism involving domain wall displacement, as it is clearly shown for the ML surface in Fig. 13(a).

### G. Depth-dependent switching

Summarizing the results discussed above we are led to the following conclusion: the layers in the vicinity of the surface switch at higher fields (up to a factor of 4, see Fig. 12) than the bulk of the ML. Neither the thickness $t$ nor the magnetization $M$ of the magnetic components described by Eq. (2) can change $H_{afm}$ to this extent. However, the bilinear coupling strength $J_{bil}$ is known to depend very strongly on small changes of the spacer thickness. Calculations in Ref. 32 suggest that topological roughness (lateral fluctuations of the number of spacer lattice planes) may change the value of $J_{bil}$ by an order of magnitude or more. Likewise, GMR measurements on Cu/Co MLs, e.g., in Ref. 33 revealed that Cu spacer thickness variations in the range of some tenths of an angstrom cause large changes in the coupling strength without affecting the high GMR values. Therefore, already a very small gradient of the spacer thickness and/or roughness toward the surface of the ML may be sufficient to explain the measured $J_{bil}$ increase.

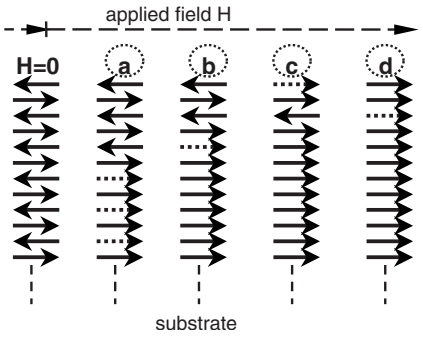


FIG. 15. Model of subsequent layer switching of the layer stack from the afm state to the fm saturated state in quadrant 4 (ascending branch) of the loops (see Figs. 11–13, compare especially the encircled letters). The actual switching layer is dotted (see text).

Based on the above discussion and the results of Figs. 11–13, we propose a model for the switching of the layer stack as shown in Fig. 15 for the case of a field applied along the easy axis, starting from the afm-coupled state (in remanence) and proceeding to the saturated state, i.e., following the ascending branches in Figs. 11, 12, and 13(a). The encircled letters correspond to the steps in the figures mentioned and the spin structure changes in every step are marked by dotted arrows in Fig. 15. At first, the interior of the layer stack switches, which can only be observed in the GMR signal and the volume magnetization. From Fig. 11 one can estimate that ~75% of the ML are involved in this process. The previously discussed increase of the switching fields toward the surface is not found for the top magnetic layer: because of the afm coupling to only one adjacent layer the switching field of the outermost layer is strongly reduced. The one-sided coupling is discussed in Ref. 2 to create a spin-flop reversal of the surface layer of a ML with an even number of magnetic layers: This surface spin flop should occur[2] as follows: "…at a field lower than that appropriate to the infinite structure by roughly a factor of $\sqrt{2}$ in the limit in which the anisotropy is small compared to the exchange…," i.e., $H_K \ll H_{afm}$ [see Eqs. (1) and (2)]. The results presented here prove for the case $H_K > H_{afm}$ a spin flip for the surface layer also at a lower field than for the adjacent fm layer (here odd magnetic layers).

For fields decreasing from the saturation state the situation is more complex and cannot be presented as simple as in Fig. 15 for the increasing field. For instance, the magnetization change at step c in Fig. 11 seems to split into the two steps f and g (which eventually indicates two flop processes) and the counterpart of step b is hidden in step h (all letters referring to the highest temperature) ($T$=400 K) ascending and descending branches in Fig. 11, where the steps are most pronounced. After the field decreases to $H$=0 we reach the remanent state for the descending branch. Now every magnetic layer has changed its magnetization direction by 180° as can be inferred from the magnetization and MOKE loops in Fig. 12. If we assume a nearly symmetric switching of the

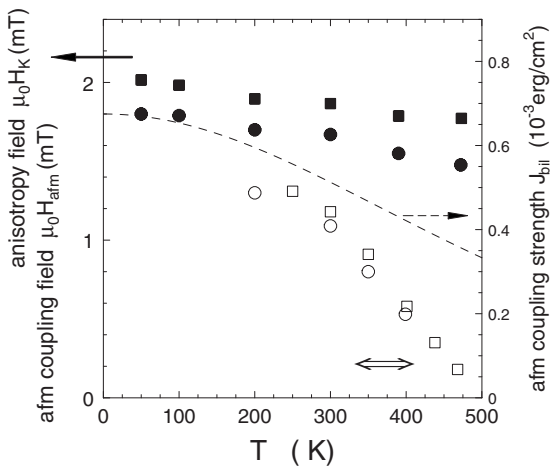


FIG. 16. Temperature dependence of the anisotropy field $H_K$ (filled symbols, see Table I with Fig. 1) and the afm coupling field $H_{afm}$ of the bulk of the ML stack [(open squares) GMR values, (open circles) magnetization loops; see Figs. 8–10]. The right-hand $y$ scale is computed from Eq. (2) for the actual layer stack, showing the extremely low value of the coupling strength. The dotted line shows the temperature damping of ideal Ruderman-Kittel-Kasuya-Yosida coupling, adapted with parameters of our ML, see text.

surface layers on both sides of the layer stack, the magnetization change, e.g., of step c in Fig. 11, is in satisfactory agreement with the value of the saturation magnetization (a 180° change of 2 out of 41 magnetic layers makes up for about 10% magnetization change as in the figure).

### H. Temperature dependence of $H_K$ and $H_{afm}$

In Fig. 16 we display the temperature dependences of the afm coupling field strengths $H_{afm}$, as derived from GMR (open squares) and magnetization measurements (open circles). The values are taken from Figs. 8 and 10—averaged for the distinct branches—as the field strengths corresponding to the highest slopes, discussed above as the afm coupling fields for the bulk of the ML stack. Below room temperature this procedure becomes more and more impracticable. Additionally, the anisotropy fields for the neighboring fm-coupled combs, collected in Table I, are plotted. They should represent the anisotropy of the afm-coupled comb e in between (see Fig. 1).

The temperature dependence of the interlayer coupling $J$ according to a Ruderman-Kittel approach after Refs. 32 and 34 is caused by the rounding of the Fermi-Dirac function as $J \propto J_0[z/L(T)]/[\sinh(z/L(T))]$ with $z$ being the spacer thickness and $L(T) \propto 1/T$ an attenuation length. Taking the Cu spacer thickness from Fig. 1 as 22 Å and a value of $L(300\ \mathrm{K}) = 16.7$ Å for the (111) direction from Ref. 32, the dotted line in Fig. 16 gives the temperature dependence for an arbitrary constant $J_0$ in case of an ideally smooth spacer. On the other hand, we observe a much stronger decrease of the coupling strength. We should keep in mind, however, that *a priori* a constant $J_0$ value cannot be taken for granted, because of—among other things—the saturation magnetization decreasing with $T$ (see Fig. 7). Additionally, even the thermal expansion (spacer thickness increase ≈0.2 Å for $\Delta T = 500$ K) in combination with the aliasing effect can decrease the coupling, especially in the right flank of the second afm coupling maximum [see Fig. 2(b) in Ref. 32].

Figure 16 suggests that for low temperatures the anisotropy field $H_K$ and the afm coupling field $H_{afm}$ are in the same range. With increasing temperature the ratio $H_K/H_{afm}$ strongly increases. This is the key for interpreting the measured effects, shown in Figs. 8–11: the increasing ratio $H_K/H_{afm}$ causes the ML to switch more and more steplike. In this way, we arrive at a spin-flip transition involving nucleation processes and domain wall propagation, as it is theoretically discussed in Ref. 1 to occur in real systems without hysteresis. The experimentally observed continuous approach to the pronounced spin-flip transition with a strong increase of the ratio $H_K > H_{afm}$, however, is in strong contrast to the prediction of a sharp transition at a relatively low value $H_K/H_{afm} \approx 1$ (as predicted in Ref. 1). This discrepancy can be explained by the fact that the estimated $H_K$ values (collected in Table I) are averaged values over the entire sample which can include a direction distribution of the local $H_K$ values, too.

## IV. SUMMARY AND CONCLUSIONS

Combined measurements of the magnetization, GMR, MOKE, including Kerr microscopy studies allowed us to elucidate the detailed mechanism of the afm-fm transition in an applied field for the bulk and the surface layers of a NiFe/Cu multilayer stack. We find that the ratio of the anisotropy field $H_K$ and the afm coupling field $H_{afm}$ is decisive for the type of transition that takes place in an applied field along the easy axis. The strong difference in the temperature variations of the intralayer magnetic anisotropy (almost temperature independent) and the afm coupling strength (strong decrease with temperature) provides a handle to change the ratio $H_K/H_{afm}$ by more than an order of magnitude for one and the same multilayer in the temperature range $T < 500$ K. For $H_K \gg H_{afm}$ at high temperatures the transition afm⇔fm takes place by a sharp steplike switching, visible in both the GMR and magnetization curves. This switching is related to a spin-flip transition, realized by domain nucleation and domain wall propagation. This is confirmed for the surface of the ML by direct observations via Kerr microscopy. For the bulk of the ML this mechanism is concluded on the basis of magnetic viscosity effects in the GMR, and is additionally supported by a linear GMR dependence on the net magnetization. On the other hand, for applied fields along the hard axis magnetization rotation processes are observed by Kerr microscopy and the GMR is found to depend quadratically on the magnetization.

We also show that in the considered domain wall displacement regime the surface layer switches at lower fields than the adjacent one, as it is already discussed in literature for the spin-flop switching model.

With decreasing temperature the ratio $H_K/H_{afm}$ decreases, causing a drastic change in the shape of GMR and magnetization characteristics. The steps are washed out and a transition from domain wall displacement to magnetization

canting or rotation, i.e., in direction to spin-flop behavior, occurs. At the lowest temperatures the coercivity of the ML dominates the GMR and magnetization loops and only the amplitude, but not the shape of the loops resembles the GMR-type characteristics.

**ACKNOWLEDGMENTS**

The engaged collaboration of I. Kiwitz is gratefully acknowledged. The authors thank L. van Loyen for the preparation of the samples and useful discussions.

*Author to whom correspondence should be addressed; d.elefant@ifw-dresden.de

[1] B. Dieny, J. G. Gavigan, and J. P. Rebouillat, J. Phys.: Condens. Matter **2**, 159 (1990); B. Dieny and J. P. Gavigan, *ibid.* **2**, 187 (1990).
[2] R. W. Wang, D. L. Mills, Eric E. Fullerton, J. E. Mattson, and S. D. Bader, Phys. Rev. Lett. **72**, 920 (1994).
[3] S. G. E. te Velthuis, J. S. Jiang, S. D. Bader, and G. P. Felcher, Phys. Rev. Lett. **89**, 127203 (2002).
[4] F. C. Nörtemann, R. L. Stamps, A. S. Carrico, and R. E. Camley, Phys. Rev. B **46**, 10847 (1992).
[5] D. L. Mills, Phys. Rev. Lett. **20**, 18 (1968); W. Saslow and D. L. Mills, Phys. Rev. **171**, 488 (1968).
[6] V. Lauter-Pasyuk, H. J. Lauter, B. P. Toperverg, L. Romashev, and V. Ustinov, Phys. Rev. Lett. **89**, 167203 (2002).
[7] M. Rührig, R. Schäfer, A. Hubert, R. Mosler, J. A. Wolf, S. Demokritov, and P. Grünberg, Phys. Status Solidi A **125**, 635 (1991).
[8] N. S. Almeida and D. L. Mills, Phys. Rev. B **52**, 13504 (1995).
[9] K. Pettit, S. Gider, S. S. P. Parkin, and M. B. Salamon, Phys. Rev. B **56**, 7819 (1997).
[10] G. Binasch, P. Grünberg, F. Saurenbach, and W. Zinn, Phys. Rev. B **39**, 4828 (1989).
[11] M. T. Johnson, S. T. Purcell, N. W. E. McGee, R. Coehoorn, J. aan de Stegge, and W. Hoving, Phys. Rev. Lett. **68**, 2688 (1992); M. T. Johnson, R. Coehoorn, J. J. de Vries, N. W. E. McGee, J. aan de Stegge, and P. J. H. Bloemen, *ibid.* **69**, 969 (1992).
[12] G. Reiss, L. van Loyen, T. Lucinski, D. Elefant, H. Brückl, N. Mattern, R. Rennekamp, and W. Ernst, J. Magn. Magn. Mater. **184**, 281 (1998).
[13] J. McCord, T. Schmitte, R. Schäfer, R. Zabel, and L. Schultz, IEEE Trans. Magn. **39**, 2687 (2003).
[14] R. Schäfer, J. Magn. Magn. Mater. **148**, 226 (1995).
[15] R. Schäfer, A. Hubert, and S. S. P. Parkin, IEEE Trans. Magn. **29**, 2738 (1993).
[16] Yiming Huai, Minshen Tan, and R. Rottmayer, IEEE Trans. Magn. **34**, 918 (1998).
[17] L. van Loyen, D. Elefant, D. Tietjen, C. M. Schneider, M. Hecker, and J. Thomas, J. Appl. Phys. **87**, 4852 (2000).
[18] M. Hecker, D. Tietjen, H. Wendrock, C. M. Schneider, N. Cramer, L. Malkinski, R. E. Camley, and Z. Celinski, J. Magn. Magn. Mater. **247**, 62 (2002).
[19] J. C. Slonzcewski, IEEE Trans. Magn. **MAG-4**, 15 (1968).
[20] S. Chikazumi, *Physics of Magnetism* (Krieger, Malabar, FL, 1978), p. 405.
[21] H. Katada, T. Shimatsu, I. Watanabe, H. Muraoka, Y. Sugita, and Y. Nakamura, IEEE Trans. Magn. **36**, 2905 (2000).
[22] S. Chikazumi, *Physics of Ferromagnetism* (Clarendon, Oxford, 1997), p. 256.
[23] *Ultrathin Magnetic Structures*, edited by J. A. C. Bland and B. Heinrich (Springer-Verlag, Berlin, 1994), Vol. 1, p. 74.
[24] J. A. Osborn, Phys. Rev. **67**, 351 (1945).
[25] K.-H. Müller, in *Encyclopedia of Materials: Science and Technology* (Elsevier Science, New York, 2001), pp. 4997–5004.
[26] S. Chikazumi, *Physics of Ferromagnetism* (Ref. 22), p. 548.
[27] A. Chaiken, G. A. Prinz, and J. J. Krebs, J. Appl. Phys. **67**, 4892 (1990).
[28] B. Dieny, V. S. Speriosu, S. S. P. Parkin, B. A. Gurney, D. R. Wilhoit, and D. Mauri, Phys. Rev. B **43**, 1297 (1991).
[29] R. Weber and P. E. Tannenwald, J. Phys. Chem. Solids **24**, 1357 (1963).
[30] D. Elefant, D. Tietjen, L. van Loyen, I. Mönch, and C. M. Schneider, J. Appl. Phys. **89**, 7118 (2001).
[31] G. Träger, L. Wenzel, and A. Hubert, Phys. Status Solidi A **131**, 201 (1992).
[32] P. Bruno and C. Chappert, Phys. Rev. Lett. **67**, 1602 (1991).
[33] *Metal Based Thin Films for Electronics*, edited by K. Wetzig and C. M. Schneider (Wiley-VCH, Weinheim, 2003), p. 264.
[34] P. Bruno and C. Chappert, Phys. Rev. B **46**, 261 (1992).